PLOS | COMPUTATIONAL BIOLOGY

RESEARCH ARTICLE

# A Looping-Based Model for Quenching Repression

**Yaroslav Pollak[1,2], Sarah Goldberg[1], Roee Amit[1,2]***

**1** Biotechnology and Food Engineering, Technion - Israel Institute of Technology, Haifa, Israel, **2** Russell Berrie Nanotechnology Institute, Technion - Israel Institute of Technology, Haifa, Israel

* roeeamit@technion.ac.il



OPEN ACCESS

**Citation:** Pollak Y, Goldberg S, Amit R (2017) A Looping-Based Model for Quenching Repression. PLoS Comput Biol 13(1): e1005337. doi:10.1371/journal.pcbi.1005337

**Editor:** Alexandre V Morozov, Rutgers University, UNITED STATES

**Received:** November 14, 2016

**Accepted:** December 29, 2016

**Published:** January 13, 2017



**Data Availability Statement:** All relevant data are within the paper and its Supporting Information files.

**Funding:** This project was funded by the European Union's Horizon 2020 Research And Innovation Programme under grant agreement 664918—MRG-GRammar (https://ec.europa.eu/programmes/horizon2020/), and by the Israel Science Foundation through grant 1677/12 (https://www.isf.org.il/). The funders had no role in study design, data collection and analysis, decision to publish, or preparation of the manuscript.

## Abstract

We model the regulatory role of proteins bound to looped DNA using a simulation in which dsDNA is represented as a self-avoiding chain, and proteins as spherical protrusions. We simulate long self-avoiding chains using a sequential importance sampling Monte-Carlo algorithm, and compute the probabilities for chain looping with and without a protrusion. We find that a protrusion near one of the chain's termini reduces the probability of looping, even for chains much longer than the protrusion–chain-terminus distance. This effect increases with protrusion size, and decreases with protrusion-terminus distance. The reduced probability of looping can be explained via an eclipse-like model, which provides a novel inhibitory mechanism. We test the eclipse model on two possible transcription-factor occupancy states of the *D. melanogaster eve* 3/7 enhancer, and show that it provides a possible explanation for the experimentally-observed *eve* stripe 3 and 7 expression patterns.

## Author Summary

Biological regulation-at-a-distance, whereby a transcription factor (TF) is able to generate susbstantial regulatory effects on gene expression even though it may be bound a large distance away from its target (500 bp–1 Mbp), is only partially understood. Using a biophysical model and a computer simulation that take dsDNA and TF volumes into account, we identify a downregulatory mechanism which functions at large distances, whereby a TF bound within ∼ 150 bp from an activator decreases the probability of looping-based interaction between the activator and the distant core promoter. This "eclipse" mechanism provides insight into the question of how enhancer architecture dictates gene expression.

## Introduction

Polymer looping is a phenomenon that is critical for the understanding of many chemical and biological processes. In particular, DNA looping has been implicated in transcriptional regulation across many organisms, and as a result plays a crucial role in how organisms develop and respond to their environments. While DNA looping has been studied extensively over the last

**Competing Interests:** The authors have declared that no competing interests exist.

several decades both experimentally [1–5] and theoretically [6–11], many aspects of looping-based transcriptional regulation remain poorly understood.

*In vivo*, the simplest looping-based regulatory architecture is comprised of a protein, or activator, that interacts with a distal site via DNA looping. Such simple architectures can be found in bacteria, where, for example, $\sigma^{54}$ ($\sigma^{N}$) promoters are activated via such a mechanism [12–14]. In eukaryotes, DNA-looping-based regulation is associated with the interaction between the core promoter and distal regulatory regions called enhancers. These $\sim$500 bp enhancers typically contain clusters of transcription factor (TF) binding sites, and may be located from 1 kbp to several Mbps away from their regulated promoters. Detailed studies of enhancers from several organisms [15] have revealed that TFs can upregulate, inhibit, or both upregulate and inhibit gene expression via a variety of mechanisms. For example, repressors like *D. melanogaster* Giant, Knirps, Krüppel, and Snail inhibit expression either by partial overlap of their binding sites with that of an activator, or via a short-range repression mechanism termed "quenching", whereby TFs positioned several tens of bps either upstream or downstream from the nearest activator inhibit gene expression [16–19].

In quenching, a bound protein inhibits gene expression, apparently without any direct interaction between the protein and either the promoter or the nearest-bound activator. In the prevailing model, quenching is assumed to be a result of histone deacetylation, which is facilitated by the formation of a $\sim$450 kDa DNA-bound chromatin remodeling complex made of a DNA-binding protein such as Knirps, C-terminus binding protein (CtBP) [20–22], and the histone deacetylases (HDACs) Rpd3 [23] and Sin3 [24]. However, this model falls short of providing a full description of quenching. In particular, short-range repressors such as Knirps have been shown to retain a regulatory function even without the CtBP binding domain [22, 25, 26], and tests for HDAC activity using either Rpd3 knock-outs [27] or the HDAC inhibitor trichostatin A failed to alleviate the observed repression effects [26]. Consequently, the mechanistic underpinnings of quenching are still poorly understood.

Previously, we studied looping-based regulatory mechanisms for synthetic bacterial enhancers, in which the activator was bound close to the promoter (within $\sim$1 Kuhn length, or $\sim$300 bp) [28]. We successfully modeled the experimental results using a modified worm-like chain model that takes excluded-volume considerations into account [29–31]. We found that the regulatory effects are maximal for TFs bound at the center of the looping segment (delimited by the activator and the promoter), and decrease as the looping segment length is increased.

In this report, we focus on regulation for looping segments much longer than the Kuhn length, which are more typical for eukaryotic enhancers. In this case, the elastic regulatory effects that we observed previously are negligible. Using the modified worm-like chain model, we show that the excluded volumes of DNA and a TF bound within $\sim$1 Kuhn length ($\sim$300 bp) either upstream or downstream of one of the loop termini can block the "line-of-sight" of the other terminus, generating an eclipse-like effect, which reduces the probability of looping. Unlike the elastic effects that we reported previously, this eclipse-like effect is independent of looping-segment length for sufficiently long looping segments. Thus, our model offers a looping-based mechanistic model for quenching repression.

## Materials and Methods

### Theoretical model

**DNA in the absence of bound proteins.** We model the DNA as a discrete semi-flexible chain made of $N$ individual links of length $l$. A chain is described by the locations $\mathbf{r}_i$ of its link ends, and a local coordinate system defined by three orthonormal vectors $\hat{u}_i$, $\hat{v}_i$, $\hat{t}_i$ at each link,

where $\hat{t}_i$ points along the direction of the $i$th link. We use the following notations for a specific chain configuration: $\theta_i$, $\phi_i$ are the zenith and azimuthal angles of $\hat{t}_i$ in local spherical coordinates of link $i-1$, respectively. $\{\theta,\phi\}_n \equiv \{\theta_1,\ldots,\theta_n,\phi_1,\ldots,\phi_n\}$ denotes all the angles until link $n$. Joint $i$ is the end-point of link $i$ and joint 0 is the beginning terminus of the chain. $w$ is the effective cross-section of the polymer. Each chain joint is engulfed by a "hard-wall" spherical shell of diameter $w$. The total elastic energy associated with the polymer chain can be written as follows [29]:

$$E(\{\theta,\phi\}_N) = \sum_{i=2}^{N} E^{\text{bend}}(\theta_i,\phi_i) + \sum_{i=2}^{N} E_i^{\text{hw}}\left(\{\theta,\phi\}_i\right), \tag{1}$$

where the elastic contribution to the energy is given by:

$$\beta E^{\text{bend}}(\theta_i,\phi_i) = a(1-\cos\theta_i), \tag{2}$$

$a$ is the bending constant of the polymer chain, and we have assumed azimuthal symmetry. The hard-wall contribution is given by:

$$\beta E_i^{\text{hw}}\left(\{\theta,\phi\}_i\right) = \begin{cases} \infty & i \text{ overlaps with one or more} \\ & \text{joints } 0\ldots(i-\Delta i) \\ 0 & \text{otherwise} \end{cases}. \tag{3}$$

Here $\beta = (k_b\,T)^{-1}$, $k_b$ is the Boltzmann factor and $T$ is the temperature. In case $l \geq w$, $\Delta i = 1$. In case $l < w$, two or more consecutive spheres overlap and $\Delta i$ ensures that links $j$ and $k$ interact only if $|j-k| \geq \Delta i \geq \frac{w}{l}$. For simplicity, we disregard the contribution of the twist degree of freedom to the elastic energy in this work (see discussion in S1 File Section 1.1).

**DNA in the presence of bound proteins.** We model the bound proteins as hard-wall spherical protrusions positioned adjacent to the polymer chain, with radius $R_o$ representative of the protein's volume (Fig 1). Since we neglect torsion effects in our present model, there is no intrinsic rotation of $\hat{u}_i$ around the polymer axis. Thus, we define the orientation of the bound proteins by rotating $\hat{u}_i$ around $\hat{t}_i$. Therefore, the center of a protrusion bound to chain link $k$ and rotated around the chain axis by an angle of $\gamma_k$ is given by:

$$\mathbf{r}_{\text{object}} = \mathbf{r}_k + \left(\frac{w}{2} + R_o\right)\mathbf{R}(\gamma_k,\hat{t}_k)\hat{u}_k, \tag{4}$$

where $\mathbf{R}(\gamma_k,\hat{t}_k)$ is a rotation matrix by an angle $\gamma_k$ around $\hat{t}_k$ (see Fig 1). Addition of a protrusion at link $k$ slightly alters Eq (3), requiring to test whether joint $i$ overlaps with one or more joints $0\ldots(i-\Delta i)$ and with the protrusion at $\mathbf{r}_{\text{object}}$, if $i > k$.

**Definition of looping probability ratio.** We consider a chain looped if $\mathbf{r}_N$ is confined to a volume $\delta\mathbf{r}$ around $\mathbf{r}_0$ (see Fig 1), defined by:

1. $d_{\min} \leq |\mathbf{r}_N - \mathbf{r}_0| \leq d_{\min} + \varepsilon$.
2. $(\mathbf{r}_N - \mathbf{r}_0)$ is collinear with $\hat{u}_0$ within $\delta\omega'$.

Although these criteria describe looping of chain ends, we also considered the case of looping between two inner chain sites (see Section Looping at chain ends vs. looping in the middle of the chain).

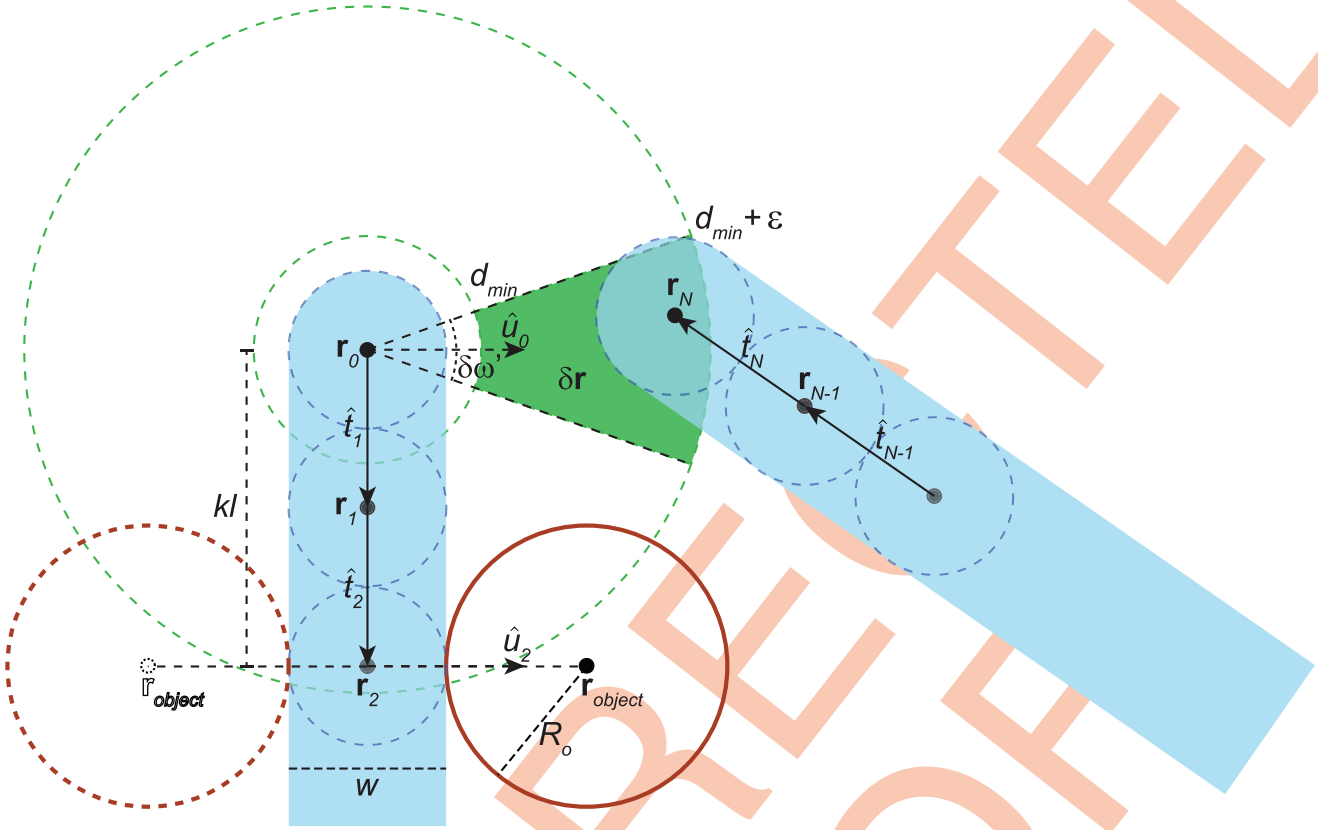


**Fig 1. Loop and protrusion geometry.** The chain (shaded in cyan) is modeled by spheres (blue dashed circles), here with link length $l$ equal to diameter $w$. Chain joint locations are marked as $\mathbf{r}_i$, for $i = 0, \ldots, N$. Arrows along chain links indicate orientations $\hat{t}_i$. The green wedge depicts the cross-section of the looping volume $\delta\mathbf{r}$ that is coplanar with looping volume orientation $\hat{u}_0$. The protrusion is positioned on the second link ($k = 2$). In-phase-with-$\hat{u}_0$ ($\gamma_2 = 0^\circ$) and out-of-phase ($\gamma_2 = 180^\circ$) positions are illustrated by the solid and dashed red circles, respectively. In this schematic representation, all chain joints are depicted in the 2D plane defined $\hat{u}_0$.

doi:10.1371/journal.pcbi.1005337.g001

For a specific choice of $\delta\mathbf{r}$, we define the probability of a polymer chain of length $L$ to form a loop as [29]:

$$P_{\text{looped}}(L) \equiv \int_{\delta\mathbf{r}} \mathbf{C}(\mathbf{r})\mathrm{d}\mathbf{r}, \tag{5}$$

where $\mathbf{C}(\mathbf{r})$ is the probability density function of the end-to-end vector $\mathbf{r} \equiv \mathbf{r}_N - \mathbf{r}_0$. In this work we study the effect of a bound object on the probability of the polymer to form a loop, with the looping criteria defined above. We quantify this effect by the looping probability ratio:

$$F(L, \text{object}) \equiv \frac{P_{\text{looped}}^{\text{object}}(L)}{P_{\text{looped}}^{\text{baseline}}(L)}, \tag{6}$$

where $P_{\text{looped}}^{\text{baseline}}(L)$ is the looping probability of the bare polymer chain and $P_{\text{looped}}^{\text{object}}(L)$ is the looping probability of the polymer chain with a protrusion bound to it.

## Simulation

Linear polymers have been studied via simulations using a variety of methods [32, 33]. To model DNA fully it is necessary to take into account the experimentally observed non-

entangled chromosomal DNA structure [34], and to include details regarding bound proteins. Recently, polymer rings have been studied as a model system for topologically constrained polymer melts, such as chromosomal DNA [35, 36]. In this work, we address looping of a linear polymer, neglecting the additional topological constraints, but including bound protrusions. We chose to simulate a linear DNA chain with a bound protein using a sequential importance sampling Monte-Carlo approach that we used previously to simulate the configurational space of bare DNA [29]. To adapt our algorithm to the case of protein-bound DNA, we take into account not only the growing chain but also the location of the protrusion (see Eq (4)). During chain generation, upon reaching link $k$, the simulation adds a hard-wall spherical protrusion with radius $R_o$ at the location $\mathbf{r}_{\text{object}}$. If the protrusion overlaps any of the previously-generated chain links or protrusions, the chain is discarded. After generating the configurational ensemble, we identify the subset of "looped" chains. We provide the essential details of the simulation in this Section. Additional details can be found in S1 File.

**Sequential importance sampling.** Our Monte-Carlo algorithm is an off-lattice sequential importance sampling algorithm adapted from a method developed by Rosenbluth and Rosenbluth [37] to generate self-avoiding walks on a lattice (as described in [29]). We generate faithful statistical ensembles consisting of $N_c \approx 10^9$ self-avoiding DNA chains with bound proteins modeled as hard-wall spheres. A chain $j$ in the ensemble is assigned with a Rosenbluth factor $w_j$ in order to negate the biasing effect introduced by sampling of self-avoiding chains. The partition function of the ensemble takes the form of

$$Z = \sum_{j=1}^{N_c} w_j, \tag{7}$$

and any physical observable can then be computed from the generated ensemble by

$$\langle f \rangle = \frac{\sum_{j=1}^{N_c} f\left(\mathbf{x}_j\right) w_j}{Z}, \tag{8}$$

where $\mathbf{x}_j$ are the generalized coordinates of configuration $j$. The probability of looping is computed by

$$P_{\text{looped}} = \left\langle f_{\text{looped}} \right\rangle, \tag{9}$$

where

$$f_{\text{looped}}\left(\mathbf{x}_j\right) = \begin{cases} 1 & \text{configuration } j \text{ is looped} \\ 0 & \text{otherwise} \end{cases}. \tag{10}$$

**Simulation parameters.** In our simulations, $d_{\min} = w$, $\varepsilon = 2w$ and $\delta\omega' = 2\pi \times 0.1$, unless stated otherwise. Changing these parameters did not alter the results significantly, and the relatively large $\varepsilon$ chosen minimized noise. We simulated the DNA chain with diameter $w = 4.6$ nm and Kuhn length [7] $b = 106$ nm, where $a$ is computed using [31]:

$$\frac{b}{l} = \frac{a - 1 + a\coth a}{a + 1 - a\coth a}. \tag{11}$$

Chains were simulated in two consecutive segments as a compromise between resolution and running time. The first $N_1$ links of the chain were simulated with link length $l_1 = 0.34$ nm,

corresponding to the length of a base-pair in dsDNA. We used $\Delta i \approx \frac{4}{3}\frac{w}{l}$ for this stage [28]. All bound objects were positioned at links $k < N_1$. The remaining $N_2$ links of the chain were simulated with link length $l_2 = w$. We denote the overall length of the chain by $L = N_1\, l_1 + N_2\, l_2$, and the distance along the chain of an object binding link $k$ from the chain origin by $K = kl_1$. We checked that this 2-stage chain generation had no effect on the resulting looping probability. For further details see S1 File, Section 1.3.

**Natural system simulation.** We modeled the structure of the *eve* 3/7 enhancer in *D. melanogaster* based on [38]. The dStat (86 kDa), Zld (146 kDa), bare Knirps (46 kDa), Knirps bound to CtBP dimers (130 kDa), and a full putative 450 kDa complex as reported by [23] were modeled as hard-wall spheres with sizes corresponding to globular proteins with radii of 3.04 nm, 3.75 nm, 2.38 nm, 3.59 nm and 5.83 nm, respectively, based on the work by [39]. Although we neglected the contribution of the twist degree of freedom to the elastic energy, we retained the twist information so that we could recreate the geometry of the *eve* 3/7 enhancer reliably. We used $2\pi/10.5$ as the DNA native twist. The chain was assumed to be rigid with respect to the twist degree of freedom. The RNA polymerase-and-cofactors complex was not modeled. Instead, for a loop to form, the chain terminus distant from the enhancer was required to be in close proximity to one of the three activators. A chain was considered looped with respect to a specific activator if it fulfilled the following conditions:

1. $d_{\min} \leq |\mathbf{r}_N - \mathbf{r}_{\text{activator}}| \leq d_{\min} + \varepsilon$.
2. $(\mathbf{r}_N - \mathbf{r}_{\text{activator}})$ is collinear with $\hat{u}_{\text{activator}}$ within $\delta\omega'$.

Here $\mathbf{r}_{\text{activator}}$ is the center of the activator sphere ($\mathbf{r}_{\text{object}}$ in Fig 1) and $\hat{u}_{\text{activator}}$ is the vector pointing from the chain axis to the center of the activator ($\hat{u}_2$ in Fig 1). We simulated DNA chains of length 3900 bp, which corresponds to the native *eve* 3/7 enhancer geometry and its separation from the *eve* promoter. The total probability of looping was computed as the sum of the looping probabilities with respect to the individual activators. In this simulation we used $d_{\min} = R_{\text{chain}} + R_{\text{activator}}$ and $\varepsilon = 3$ nm. The simulation was relatively insensitive to $\varepsilon$. For $\delta\omega'$, we chose several values: $\delta\omega' = 2\pi \times 0.1$ corresponding to a narrow cone directed away from the chain, $\delta\omega' = 2\pi$ corresponding to a full spherical shell around the activator sphere, and $\delta\omega' = -2\pi \times 0.5$ corresponding to a relatively wide cone directed towards the chain.

## Results

### Long-range down-regulatory effect

To model the quenching effect of a bound repressor on DNA looping, we generated configurational ensembles for DNA with a spherical protrusion of size $R_o = 9.2$ nm or $R_o = 18.4$ nm located a distance of $K = 95$ bp or $K = 135$ bp from the chain origin along the chain, oriented either in the same direction as the looping volume $\delta\mathbf{r}$ or 180 from it (see Fig 1). We plot $F(L)$ for the various configurations of $R_o$ and $K$ in Fig 2A. The data show that in the elastic regime ($L \leq b$), protrusions bound in-phase with $\delta\mathbf{r}$ (solid lines, ↑) strongly reduce the looping probability relative to that of the bare DNA, while protrusions positioned out-of-phase to $\delta\mathbf{r}$ (dashed lines, ↓) increase the looping probability, as we showed previously [28]. However, in the entropic regime ($L \gg b$), all chains converge to values of $F \xrightarrow{L \gg b} F_\infty \leq 1$. For protrusions that are bound in-phase (i.e. $\gamma_k = 0$), $F_\infty$ is distinctly smaller than one, and strongly depends on both the distance to the nearest terminus and the size of the protrusion. Conversely, for protrusions bound out-of-phase ($\gamma_k = 180$), $F_\infty$ is only slightly smaller than 1, with weak dependence on both protrusion size and position.

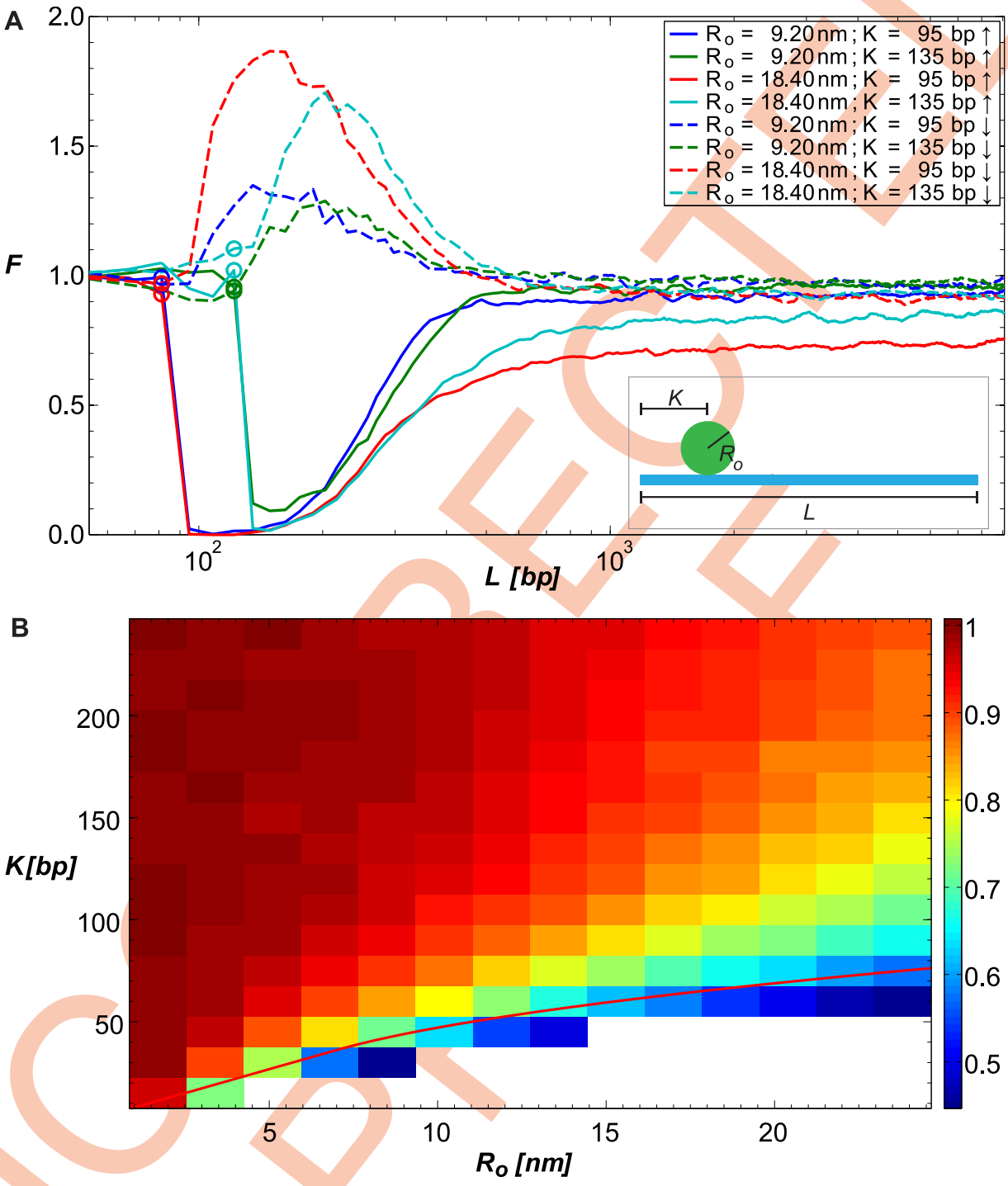


**Fig 2. Simulating looping probability ratio *F*.** (A) *F* plotted as a function of chain length *L* for several values of $R_o$ and *K*, and $\gamma_k = 0^\circ$ (solid lines) or 180° (dashed lines). The locations of the protrusions are denoted by circles on the corresponding curves. (B) $F_\infty$ plotted as a function of $R_o$ and *K*, for $\gamma_k = 0$. $F_\infty$ is calculated numerically as the average of $F(L)$ over the range of *L* values where $F(L) \approx const.$ The solid red curve is a visual aid: if the segment of the chain between the origin and the protrusion location was straight, points on the red curve would result in the protrusion touching the looping volume $\delta\mathbf{r}$.

doi:10.1371/journal.pcbi.1005337.g002

To further explore the extent of the quenching effect in the entropic or long-chain-length regime, we plot in Fig 2B the value of $F_\infty$ as a function of a wide-range of $R_o$ and $K$, for $\gamma_k = 0$. The heatmap shows both a non-linear decrease in $F_\infty$ as a function of protrusion size and a non-linear increase as a function of protrusion distance from the chain origin. The red line in the figure demarcates the closest possible location at which a protrusion can be bound without physically penetrating part of the looping volume $\delta\mathbf{r}$. Thus, for volumes and protrusion positions that fall below this line, a second excluded volume effect contributes to the reduction in the probability of looping, leading to a sharp increase in the overall effect. Together, the panels in Fig 2 show that a sufficiently-large protrusion can substantially reduce the probability of looping, independent of loop length, provided that its binding site is within a small distance from either of the loop termini. For further details regarding the computation of $F_\infty$ and its error estimation, see S1 File.

## "Eclipsing" approximation

To understand the long-range, length-independent effect shown in Fig 2, we examine the chains' terminating segments of length $T \ll L$. If $T \sim \max_{\mathbf{r}\in\delta\mathbf{r}}|\mathbf{r}-\mathbf{r}_{\text{object}}| \ll b$, these segments resemble stiff rods, and the object obstructs the line-of-sight of one chain terminus from the other. This eclipse-like phenomenon is manifested by a reduction in the number of polymer chains that are able to reach $\delta\mathbf{r}$. This, in turn, results in a smaller $P_{\text{looped}}$ as compared with the case in which no protrusion is present. In the entropic regime and in the absence of protrusions, the generated "rods" approach the looping volume $\delta\mathbf{r}$ from all directions that are unobscured by the volume of the polymer in a homogeneous fashion [7]. Due to this isotropy in the distribution of the chain termini orientations within $\delta\mathbf{r}$, the reduction in $P_{\text{looped}}$ can be approximated by the solid angle that the eclipsing object subtends at $\delta\mathbf{r}$. Consequently, $F$ (Eq (6)) can be approximated for this "rod model" by:

$$\begin{aligned} F_\infty(\tilde{\mathbf{r}}', R_o) &= \left.\frac{P^{\text{object}}_{\text{looped}}(L, \{\tilde{\mathbf{r}}', R_o\})}{P^{\text{baseline}}_{\text{looped}}(L)}\right|_{L\gg b} \\ &\approx \frac{4\pi\delta\mathbf{r} - \mathcal{I}_{\text{chain}} - \mathcal{I}_{\text{object}(\tilde{\mathbf{r}}',R_o)} + \mathcal{I}_{\text{chain}\cap\text{object}(\tilde{\mathbf{r}}',R_o)}}{4\pi\delta\mathbf{r} - \mathcal{I}_{\text{chain}}} \\ &= 1 - \frac{\mathcal{I}_{\text{object}(\tilde{\mathbf{r}}',R_o)}}{4\pi\delta\mathbf{r} - \mathcal{I}_{\text{chain}}} + \frac{\mathcal{I}_{\text{chain}\cap\text{object}(\tilde{\mathbf{r}}',R_o)}}{4\pi\delta\mathbf{r} - \mathcal{I}_{\text{chain}}}, \end{aligned} \tag{12}$$

where $R_o$ is the radius of the spherical object, $\tilde{\mathbf{r}}'$ is the location of the object, which could be located statically at point $\mathbf{r}'$ (in which case $\tilde{\mathbf{r}}' \equiv \mathbf{r}'$), or located on the chain a distance $K$ from the chain origin (in which case we use the terminology $\tilde{\mathbf{r}}' \equiv \tilde{\mathbf{r}}'(K)$ figuratively to specify the progression of the protrusion along the chain). $\mathcal{I}_{\text{chain}} \equiv \int_{\delta\mathbf{r}} \Omega_{\text{chain}}(\mathbf{r})\mathrm{d}^3\mathbf{r}$, where $\Omega_{\text{chain}}(\mathbf{r})$ is the solid angle subtended at $\mathbf{r}$ by the polymer chain links. $\mathcal{I}_{\text{object}(\tilde{\mathbf{r}}',R_o)} \equiv \int_{\delta\mathbf{r}} \Omega_{\text{object}(\tilde{\mathbf{r}}',R_o)}(\mathbf{r})\mathrm{d}^3\mathbf{r}$, where $\Omega_{\text{object}(\tilde{\mathbf{r}}',R_o)}(\mathbf{r})$ is the solid angle subtended at $\mathbf{r}$ by the object, and $\mathcal{I}_{\text{chain}\cap\text{object}(\tilde{\mathbf{r}}',R_o)}$ corresponds to the solid angle contained in both $\mathcal{I}_{\text{chain}}$ and $\mathcal{I}_{\text{object}}$.

In order to test the eclipsing hypothesis, we first computed $F_\infty$ for the case of an object statically positioned at an off-chain location $\mathbf{r}' = d\hat{u}_0$, and without chain-chain interactions. In

this simplified case, $F_\infty$ in Eq (12) can be approximated by the following eclipsing expression:

$$\begin{aligned} F_\infty(\mathbf{r}', R_o) &\approx 1 - \frac{\mathcal{I}_{\text{object}(\mathbf{r}', R_o)}}{4\pi\delta\mathbf{r}} \\ &= 1 - \frac{\int_{\delta\mathbf{r}} 2\pi \left[1 - \sqrt{1 - \left(\frac{R_o + w/2}{|\mathbf{r} - \mathbf{r}'|}\right)^2}\right] \mathrm{d}^3\mathbf{r}}{4\pi\delta\mathbf{r}} \equiv F_\infty^{\text{static}}, \end{aligned} \tag{13}$$

where we substituted

$$\frac{\Omega_{\text{object}}}{2\pi} = \int_{\sqrt{1 - \frac{(R_o + w/2)^2}{|\mathbf{r} - \mathbf{r}'|^2}}}^{1} \mathrm{d}\cos\theta = 1 - \sqrt{1 - \frac{(R_o + w/2)^2}{|\mathbf{r} - \mathbf{r}'|^2}}. \tag{14}$$

In Fig 3, we compare the value computed from Eq (13) (dashed cyan line) to $F(L)$ computed by our sequential importance sampling algorithm for the same conditions (solid blue line). The data show that the eclipsing approximation $F_\infty^{\text{static}}$ overestimates $F_\infty$. We reasoned that the main cause for this estimation error is that Eq (13) disregards the flexible polymer nature of the chain. We ran an additional Monte-Carlo simulation to quantify the correction resulting from polymer flexibility. Here, we generated pairs consisting of an end-terminus point in $\delta\mathbf{r}$ and a direction vector of the terminal link, both distributed uniformly. Short polymer chains of length $T$ originating at the chosen points were grown with their first links oriented in the chosen directions. These chains can be thought of as the terminating segments of long chains that have a uniform distribution of their end-termini in $\delta\mathbf{r}$. We found that the probability of a flexible-polymer chain to overlap the object increased relative to the probability within the "rod model", resulting in a decrease in the probability of the chain to form a loop (magenta dashed line in Fig 3). Using this "terminating-segments" correction, the discrepancy between $F_\infty$ from the simulation and $F_\infty^{\text{static}}$ from Eq 13 is partially accounted for. We attribute the additional reduction in the simulated $F_\infty$ to interactions between the object and the remaining $L - T$ length of the chain.

In Fig 4 we plot $F_\infty$ as a function of an on-chain object of radius $R_o$, for several values of $K$. To compare the results of the numerical simulation to the full eclipsing model (Eq 12), we first note that when $K$ is kept constant, $\mathcal{I}_{\text{chain}\cap\text{object}(\tilde{\mathbf{r}}', R_o)}|_{K=const} \approx const$, as can be seen from the inset in Fig 4: the overlap between $\Omega_{\text{chain}}$ (orange cones) and $\Omega_{\text{object}}$ (red cones) changes only slightly when the object grows by a factor of two. Furthermore, $|\tilde{\mathbf{r}}'(K) - \mathbf{r}|_{K=const}$ is approximately independent of $R_o$ if $(R_o + w/2) \ll |\tilde{\mathbf{r}}'(K) - \mathbf{r}|$ for all $\mathbf{r} \in \delta\mathbf{r}$. Thus, the dependence of $F_\infty$ on the radius $R_o$ of an on-chain object can be derived from Eq (12):

$$\begin{aligned} & F_\infty(\tilde{\mathbf{r}}', R_o)|_{K=const} \approx \\ \approx\ & 1 - \frac{\mathcal{I}_{\text{object}(\tilde{\mathbf{r}}', R_o)}}{4\pi\delta\mathbf{r} - \mathcal{I}_{\text{chain}}} + \frac{\mathcal{I}_{\text{chain}\cap\text{object}(\tilde{\mathbf{r}}', R_o)}}{4\pi\delta\mathbf{r} - \mathcal{I}_{\text{chain}}} \\ \approx\ & 1 - A\mathcal{I}_{\text{object}(\tilde{\mathbf{r}}', R_o)} + B_K \\ \approx\ & 1 - A_K(R_o + w/2)^2 + B_K \equiv f_K(R_o), \end{aligned} \tag{15}$$

where we approximated $\mathcal{I}_{\text{object}(\tilde{\mathbf{r}}', R_o)} \approx (R_o + w/2)^2\pi \int \frac{\mathrm{d}^3\mathbf{r}}{|\tilde{\mathbf{r}}' - \mathbf{r}|^2}$ using Eq (14) and $(R_o + w/2) \ll |\tilde{\mathbf{r}}' - \mathbf{r}|_{\mathbf{r}\in\delta\mathbf{r}}$. In Fig 4, we fit the numerical results for different values of $K$ with functions of the form $f_K(R_o)$ (Eq (15)). The fits are in excellent agreement ($R^2 \sim 0.99$) with the numerical data.

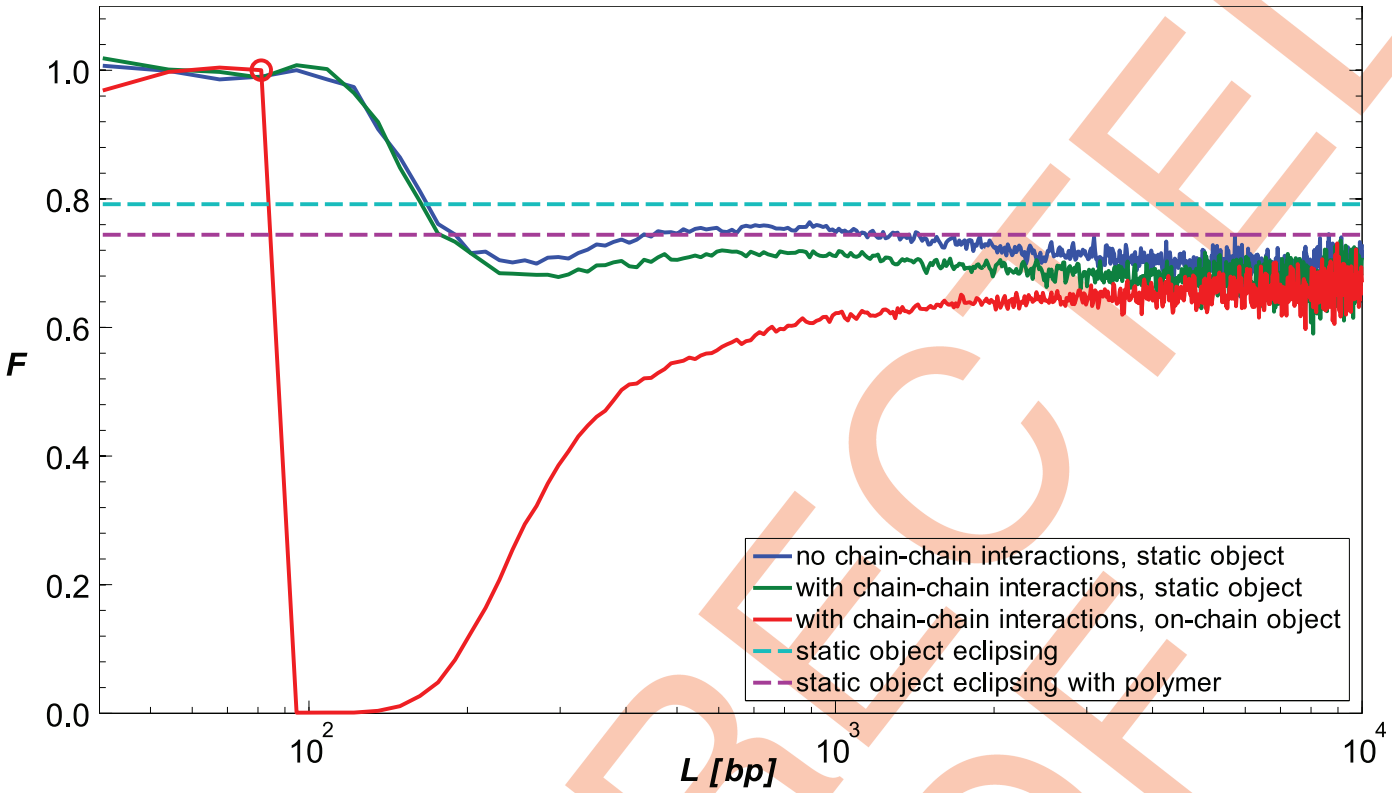


**Fig 3. Simplified eclipse models.** Simulation results for a chain without chain-chain interactions and a static object (solid blue line) are compared to estimates for $F_\infty$ of the "rod" (dashed cyan line) and "terminating-segments" (dashed magenta line) models, also for a chain without chain-chain interactions. The static object is located at $d\hat{u}_0$, where $d = 41.45$ nm, and $R_o = 23$ nm. For comparison, we plot simulation results for a chain with chain-chain interactions and the same static object parameters (solid green line), and a chain with chain-chain interaction and an on-chain object (solid read line). The on-chain object is located at $K = 94$ bp (denoted by a circle).

doi:10.1371/journal.pcbi.1005337.g003

## "Eclipsing" can occur both upstream and downstream of an activator

A salient feature of enhancers is that binding sites for TFs are positioned both upstream and downstream of the activators. The eclipse model predicts that $F_\infty(\tilde{\mathbf{r}}'(K), R_o) = F_\infty(\tilde{\mathbf{r}}'(-K), R_o)$, since for long chain lengths the correlation between the positions of both chain termini is completely abolished. Thus, from the perspective of one terminus, looping events can be initiated from any possible direction. To see if our simulation captures this symmetry, we explored a geometry in which the protein-like protrusion was positioned at negative $K$ values, corresponding to a location outside of the looping segment delimited by the looping-volume (activator) and distal-terminus (promoter) locations. To do so, we generated an additional chain segment of length $Q$ in the direction opposite to $\hat{t}_1$, starting from link 0, where $Q \gg K$. We plot the results in Fig 5. The data show that in the elastic regime, the "outside" geometry (green line, $K < 0$) generates a significantly smaller effect on the probability of looping as compared with the "inside" architecture (blue line, $K > 0$). This lack of symmetry is probably due to the propensity of short loops to form a "tear-drop" shape, thereby reducing the quenching effect of any elements bound outside the looping segment [28]. However, for sufficiently large $L/b$, $F(L)$ for both $\pm K$ enhancer geometries converge to the same value, as predicted by the eclipse model.

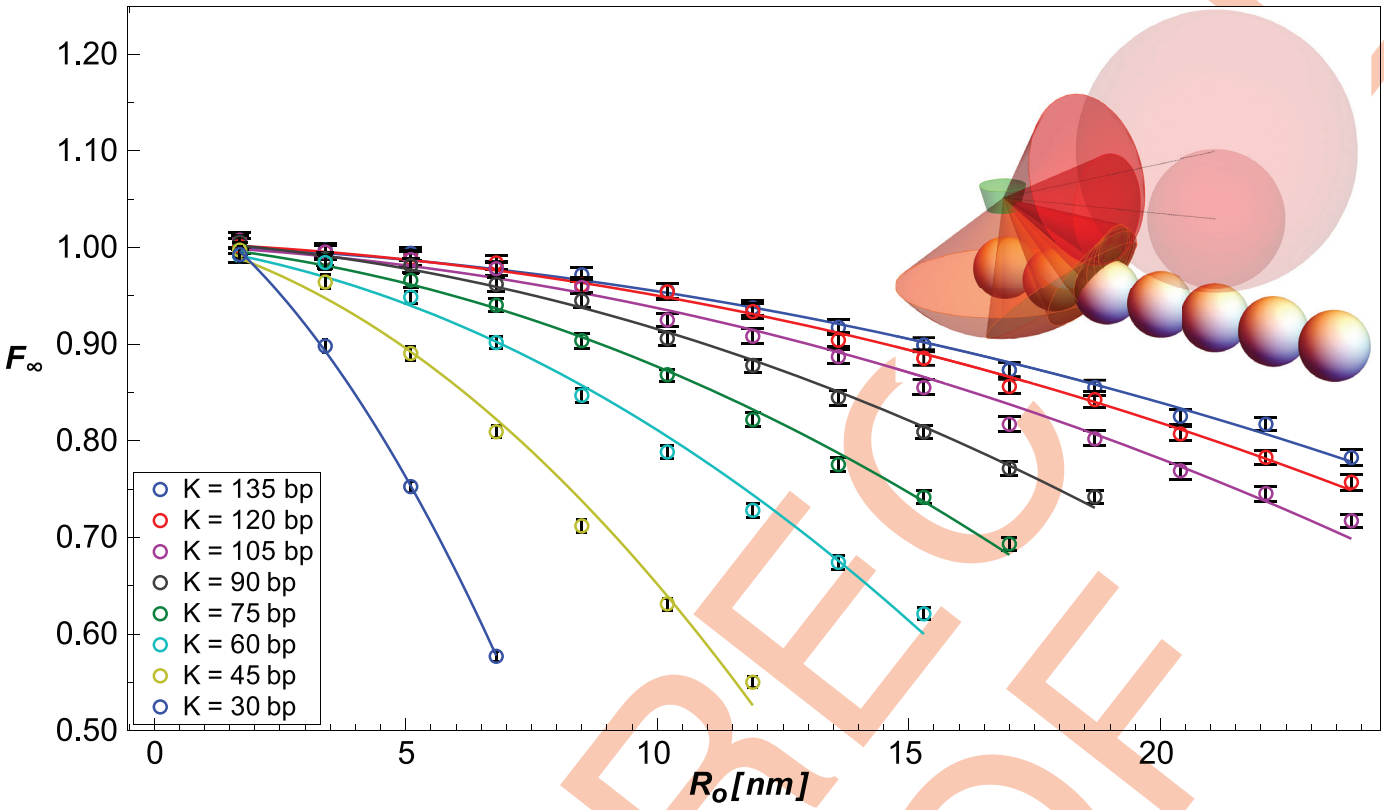


**Fig 4. Dependence of $F_\infty$ on protrusion size $R_o$.** Simulation data (circles) are fit (solid curves) by $f_K(R_o)$ (Eq 15). Data points are the mean of the last 480 points of the simulated $F$. Error bars are ±1.96 times the standard error of these points. Inset illustrates a doubling of $R_o$. $\delta\mathbf{r}$ is shown by the green volume. Chain links are shown by white spheres. Protrusions are shown by transparent red spheres. Solid angles subtended by the chain links and protrusion are shown by orange and red cones, respectively. $\Omega_{\text{chain}}$ is the area on the unit sphere around the center of $\delta\mathbf{r}$ intersecting the orange cones. $\Omega_{\text{object}}\left(\left(\tilde{\mathbf{r}}',R_o\right)\right)$ is the area on the unit sphere intersecting the red cone. $\Omega_{\text{chain}\cap\text{object}}\left(\left(\tilde{\mathbf{r}}',R_o\right)\right)$ is the area on the unit sphere intersecting both orange and read cones.

doi:10.1371/journal.pcbi.1005337.g004

## Looping at chain ends vs. looping in the middle of the chain

So far, we modeled an enhancer-promoter region by a chain of discrete semi-flexible links, with the activator and the promoter located at both ends of the chain. However, *in vivo*, the DNA chain extends far beyond the enhancer-promoter region in both directions, and is subject to confinement. We address the first issue in this section, and the issue of DNA confinement in the next section.

We computed the probability of looping for a generic loop of length $L$, located between two internal links of the chain. To do so, we extended the original length of the chain $L$ by two flanking segments of 10 Kuhn lengths ($10b$) on both ends of the chain. We assigned the cumulative Rosenbluth weight of the extended chain to the central segment of length $L$ containing the enhancer-promoter region. See S1 File, Section 1.3.

We ran a simulation with $K = 60$ bp and $R_0 = 11.9$ nm (Fig 6, magenta line) and compared $F(L)$ to the same case without flanking segments (Fig 6, blue line). The data show that there is a discrepancy in the long-range looping probability ratio between the two looping models. In particular, the down-regulatory effect of the protrusion is stronger when the enhancer-promoter region is modeled as part of a larger chain. In order to determine the individual contributions of the two flanking segments to the discrepancy, we ran additional simulations with

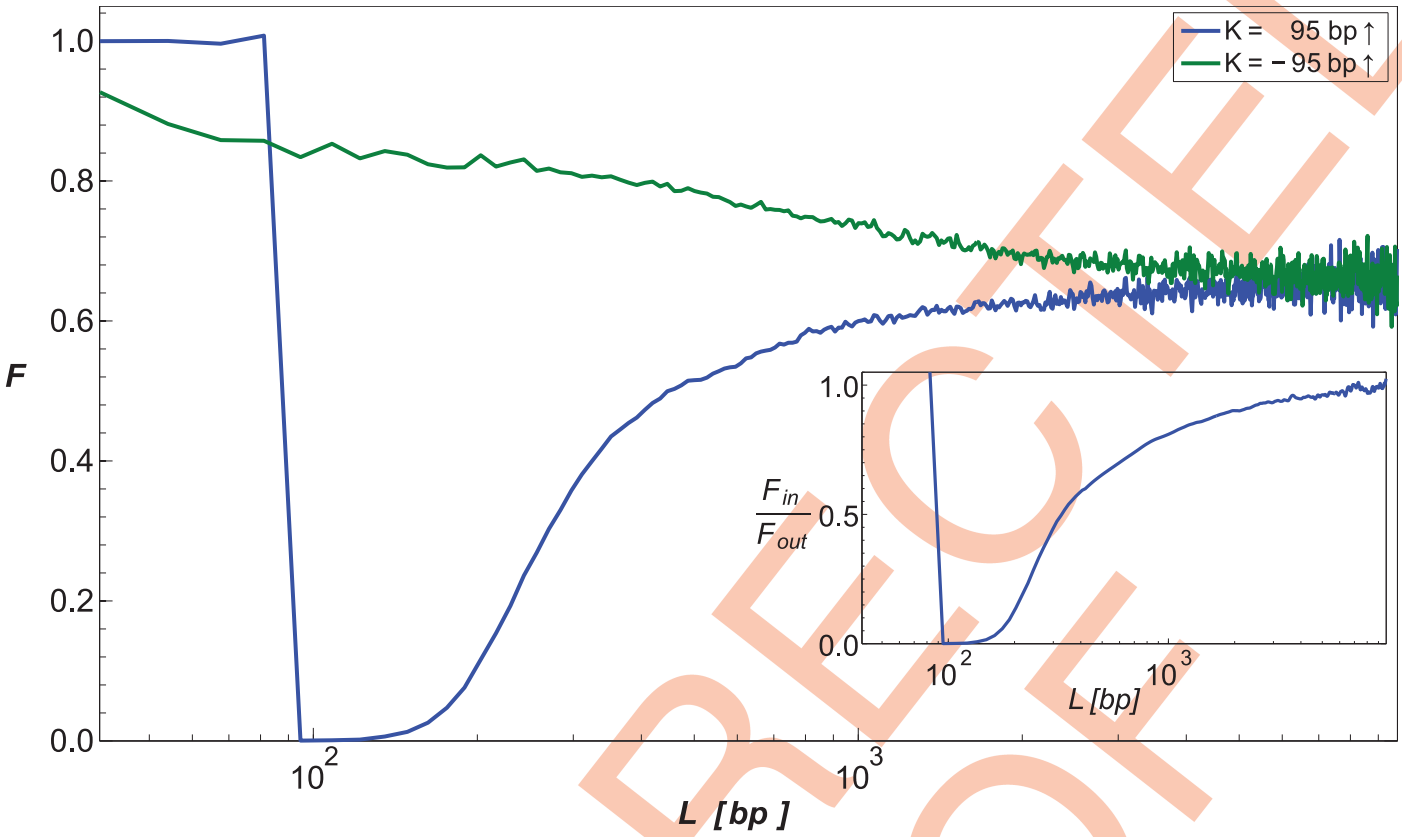


**Fig 5. Dependence of $F(L)$ on location of the protrusion.** The protrusion is located either inside ($K$) or outside ($-K$) the chain segment between link 0 and the terminating link. $R_o = 23$ nm and $K = \pm 95$ bp. Inset: the ratio $F(L, K)/F(L, -K)$.

doi:10.1371/journal.pcbi.1005337.g005

different flanking-segment configurations. We found that only the trailing segment beyond the distal terminus of the looping segment contributes to this discrepancy. The addition of a single chain link of length $w = 4.6\ nm$ ($0.092b$) after the terminus of the looping segment (Fig 6, green line) diminishes $F(L)$, accounting for approximately half of the discrepancy. The addition of only 4 links ($0.368b$) after the terminus of the looping segment (Fig 6, aqua line) accounts for the entire discrepancy, fully agreeing with the results for the case with $10b$ flanking segments on both ends of the looping segment. While an addition of a leading segment before the looping volume diminishes the looping probability (data not shown), it does not alter the looping probability ratio $F(L)$. This can be seen from the comparison between $F(L)$ for the case with a single link after the terminus of the looping segment (Fig 6, green line) and the case of a segment of length $b$ before the looping volume and a single chain link after the terminus of the looping segment (Fig 6, red line).

We believe that these results depend strongly on the looping conditions. For the conditions used here ($\delta\omega' = 0.1 \times 2\pi$, see Fig 1) the leading flanking segment is inconsequential to the looping probability ratio. However, utilizing a uniform looping volume ($\delta\omega' = 4\pi$) would lead to a diminished looping probability ratio as a result of leading segment addition. Similarly, the trailing flanking segment diminishes $F(L)$ due to the fact that chain configurations that approached the looping volume from a direction colliding with the chain are no longer possible when the chain is extended by a trailing segment. If, however, the looping conditions were such that the chain terminus was required to approach the looping volume from a direction

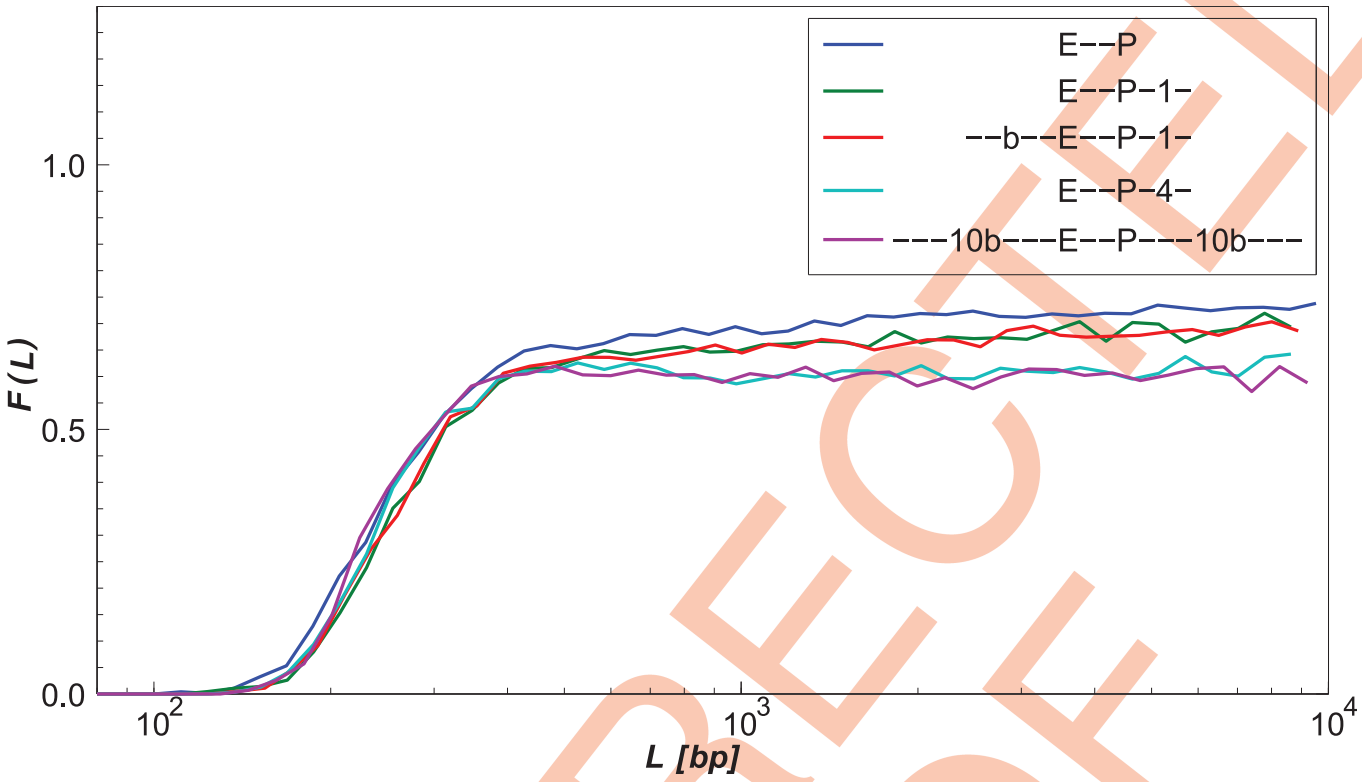


**Fig 6. Comparison of *F*(*L*) between enhancer-promoter regions with different-sized flanking segments.** All simulations ran with $K = 60$ bp and $R_0 = 11.9$ nm. Blue: No flanking segments. Green: One link $w = 4.6$ nm ($0.092b$) after the chain terminus. Red: Medium-sized segment of length $b$ before the looping volume and one link ($0.092b$) after the chain terminus. Aqua: 4 links ($0.368b$) after the chain terminus. Magenta: Long flanking segments of length $10b$ on each side of the enhancer-promoter region.

doi:10.1371/journal.pcbi.1005337.g006

perpendicular to the looping volume cone axis, the trailing segment would become inconsequential to the looping probability ratio.

These results suggest that while there is a discrepancy between the two simulation modes (with flanking regions and without them), it arises from regions that are immediately adjacent to the enhancer-promoter region, and further downstream or upstream segments of the chain do not contribute to the down-regulatory effect.

## Looping probability ratio for a confined polymer

To check the effects of polymer confinement on the looping probability, we generated chains confined by spheres of various radii (for full simulation details, see S1 File). In Fig 7, we present the normalized looping probability $P_{\text{looping}}^{\text{sphere}}/P_{\text{looping}}^{\text{free}}$ and the looping probability ratio for the confined chains, for the range of confining-sphere radii 125–625 nm. Note that the looping probability increases relative to that of the unconstrained polymer when the gyration radius of the chain becomes comparable to the size of the confining sphere (Fig 7A). However, as can be seen in Fig 7B, the introduction of a bound protrusion does not influence the looping probability ratio $F(L)$ up to a chain length of 10 kbp for confining spheres with radii $\geq$250 nm. For the smallest confining sphere (radius of 125 nm) we were only able to simulate chains of length $\leq$4.5 kbp (see S1 File Section 3.4), and here too the looping probability ratio remained unaffected.

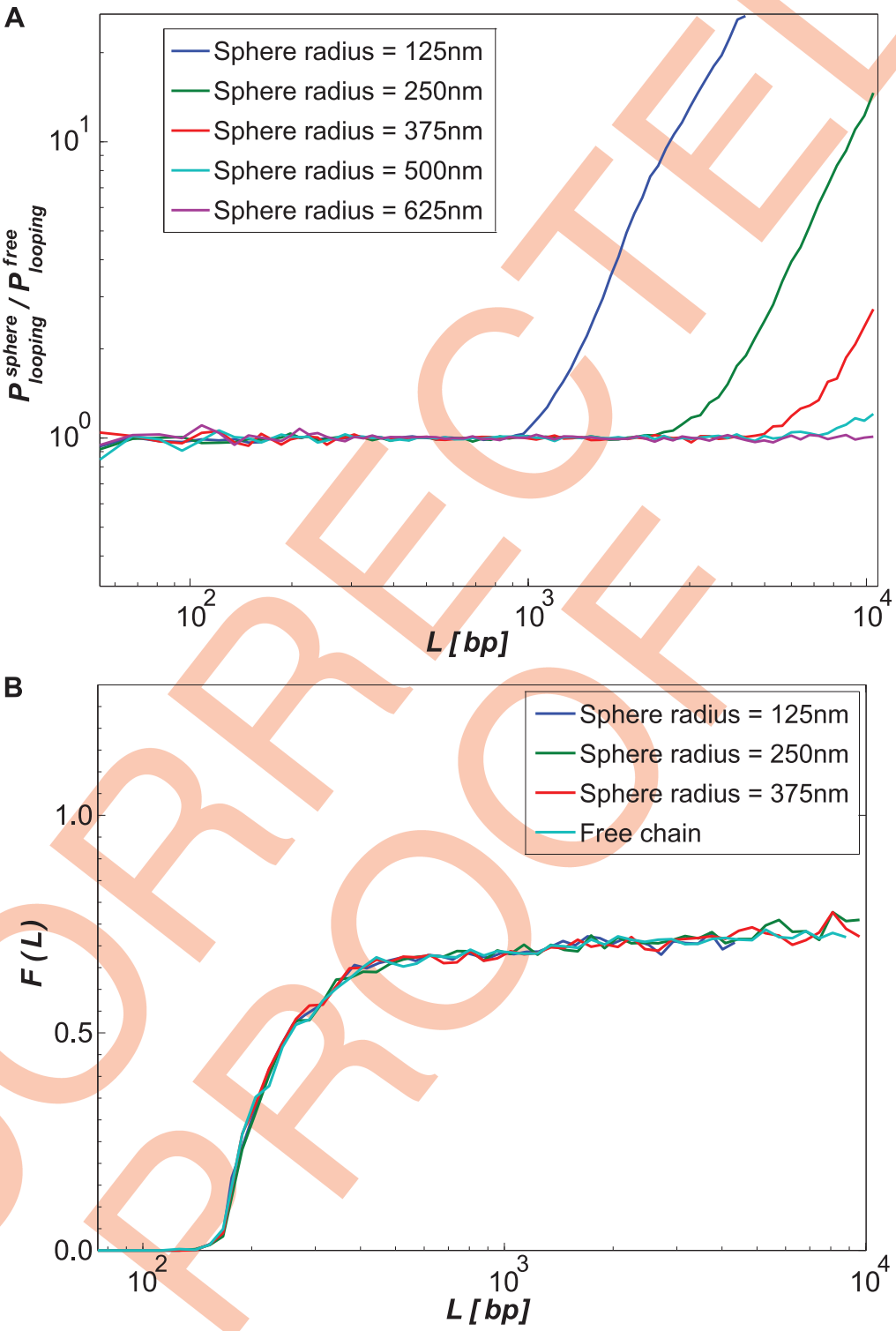


**Fig 7. Effect of a confining sphere on the probability of looping.** (A) Values of $P^{\text{sphere}}_{\text{looping}}/P^{\text{free}}_{\text{looping}}$ for various sphere sizes. (B) Values of $F(L)$ for three of the smallest spheres compared to $F(L)$ for the chain without a confining sphere.

doi:10.1371/journal.pcbi.1005337.g007

### "Eclipsing" effect for *eve* 3/7 stripe

Finally, we applied our model to a real enhancer-promoter system. We chose the experimentally well-characterized *eve* 3/7 enhancer of *D. melanogaster*, which is separated from its promoter by about 4 kbp. See Discussion for a detailed examination of the validity of this application.

We computed our model's predictions for the active *eve* 3/7 enhancer, i.e. in the early developmental stages (before gastrulation—stage 14), and in the anterior region of the *D. melanogaster* embryo. To check whether the resultant probability of looping could provide a mechanistic explanation for the observed expression pattern, we simulated two states: first, a chain representing the enhancer that is fully occupied by spherical protrusions representing the activators dStat, Zld and the Knirps repressor–co-repressor complexes, and a second state where the chain is entirely devoid of bound protrusions. We tested three possible protrusion sizes, corresponding to reported repressor complex sizes: Knirps alone (46 kDa), Knirps bound to CtBP dimers (130 kDa), and a full putative 450 kDa complex, as reported by [23]. Since the exact looping conditions of the enhancer looping are unknown, we considered three choices of $\delta\omega'$ (see Materials and Methods) that represent different extreme cases.

The results, plotted in Fig 8, show that for all chosen looping conditions, there is a decrease in the probability of looping when the chain is fully bound by the protrusion representing Knirps. However, only the protrusion representing the full Knirps–co-repressor complex (containing dCtBP and the HDACs Rpd3 [23] and Sin3 [24]) was large enough to generate a significant reduction in looping.

## Discussion

We previously established [28] that a bound protein inside a loop can alter the probability of looping in a manner proportional to its size, when the chain length is of the order of the Kuhn length (i.e. $< 300$ bp). The simulations and theory presented here identify a separate regulatory effect that is relevant to much longer chain lengths. In particular, our model predicts a decrease in the probability of looping that is independent of chain length for long chains in the entropic regime (i.e. $L \gg 300$ bp), provided that a sufficiently large protrusion oriented in-phase with the looping volume $\delta\mathbf{r}$ is positioned within one Kuhn length of one of the chain termini. We further showed that the reduction in looping probability resembles an eclipse-like phenomenon, where the protrusion blocks the line of sight of one chain terminus from the other.

Our model provides a biophysical mechanism for so-called short-range repression or quenching by enhancers, for sytems with sufficiently long separation between the enhancer and the core promoter ($L \gg b$) [16–19]. The model successfully captures many of this phenomenon's salient features. These include lack of dependence on chain length, symmetry with respect to binding-site positioning inside or outside of the looping segment, the dependence of the regulatory effect on both the size of the bound complex and the distance of the TF from the nearest terminus, and the typical distances of the TF from the terminus ($\lesssim 150$ bp) for which significant quenching can be generated.

We computed the looping probability ratio for the *D. melanogaster eve* 3/7 enhancer-promoter system in the segment of the embryo where the repressor Knirps is expressed. We found that using realistic repressor-co-repressor-HDAC complex sizes for the simulated protrusions, a significant reduction in looping probability can be obtained, showing that the looping-based mechanism can account for at least some of the quenching generated by Knirps in the context of early fly development. Since there is also a substantial body of evidence supporting HDAC catalysis as a major mechanism for repression [40], we conclude that it is likely that

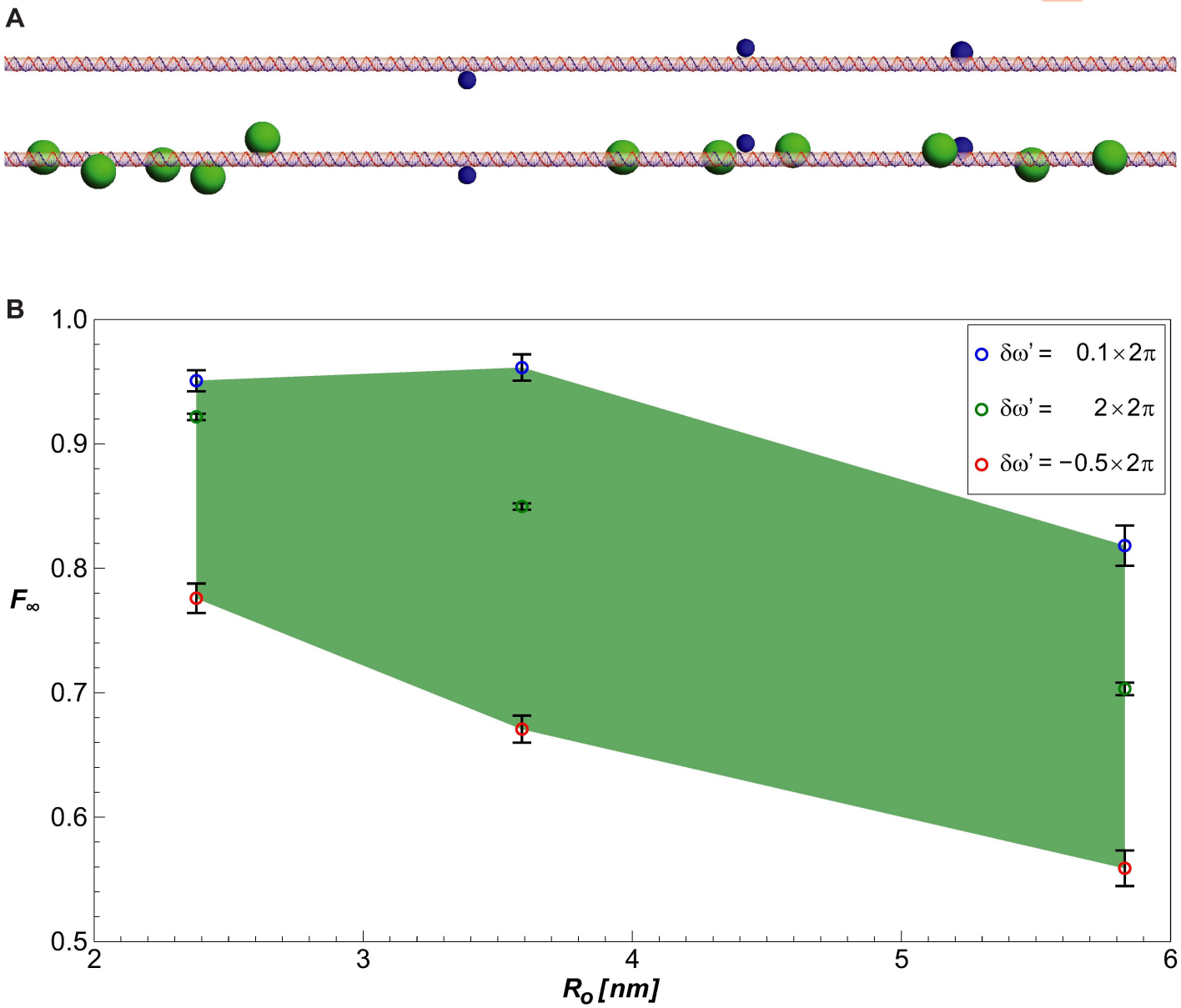


**Fig 8. Simulation of the *eve* 3/7 enhancer in *D. melanogaster*.** (A) Illustration of the *eve* 3/7 enhancer geometry with bound activators (top) vs. with both activators and full putative Knirps+dCtBP+Rpd3+Sin3 complexes (450 kDa) bound (bottom). (B) Dependence of $F_\infty$ on protrusion size $R_o$ and the looping conditions $\delta\omega'$. Negative $\delta\omega'$ corresponds to anti-collinear orientation of $(\mathbf{r}_N - \mathbf{r}_0)$ with $\hat{u}_0$. Here $d_{min} = R_{chain} + R_{activator}$ and $\varepsilon = 3$ nm. $F_\infty$ was computed from 150 simulated data points corresponding to DNA chains of lengths 3751–3900 bp. Error bars are ±1.96 times the standard error of these points. The area shaded in green depicts the range of possible $F_\infty$ values, depending on the chosen looping criteria.

doi:10.1371/journal.pcbi.1005337.g008

both HDAC activity and looping-related effects combine to generate the quenching observed in *D. melanogaster* and other organisms.

There have been previous attempts to model enhancer regulatory logic for the gap genes of early fly development [41–43]. Using a semi-empirical approach, which coupled a thermodynamic model to an empirically-based regulatory scoring function, these works demonstrated that TF occupancy of enhancers can determine the gene-expression outcome. By contrast, our model does not compute the actual expression pattern, but rather the probability of looping

for a given occupancy state. For this computation, our model requires only knowledge of the enhancer structure (TF binding sites, protein-complex sizes, and over-all enhancer-promoter distance). This implies that no gene-expression experimental data is needed as an input to predict the down-regulatory effect of bound TFs.

While this work focused on bare dsDNA with a protrusion, our results are applicable to any linear polymer as long as its length is significantly larger than its Kuhn length. However, to apply our results to chromosomal DNA, other constraints must be taken into account, some of which we attempted to address in this paper. First, natural DNA loops occur between sites within the chromosome, and not between ends. We showed that looping of a linear segment with additional upstream and downstream flanking segments qualitatively resembles looping without flanking segments. Second, chromosomal DNA is subject to confinement. Third, DNA is typically a mixture of chromatinized and non-chromatinized DNA. We adress the second and third points below.

Due to confinement, chomosomal DNA is compacted into a globular state. The nature of the globular state varies between organisms (equilibrated globule in yeast vs. a possibly non-crosslinked globule in higher eukaryotes [34, 44–46]) and chromatin spans a wide range of volume fractions [36]. For lower volume fractions, DNA can be viewed as a semi-dilute polymer solution, in which coils are strongly overlapping. This semi-dilute solution may be pictured as a system of domains (blobs). Inside each blob, the chain behaves as an isolated macromolecule with excluded volume, and different blobs are statistically independent of one another [8, 47]. If the volume fraction is sufficiently low, chromosomal DNA within a blob can explore nearly the entire volume of the blob without interacting with other parts of the chromosome. Our model is applicable to non-chromatinized dsDNA within a blob, provided that the characteristic blob size of the organism is large enough to contain a sufficiently-long length of dsDNA.

For active eukaryotic promoters, there is evidence that the enhancer and the promoter regions are depleted of nucleosomes for up to 500–1000 bp both upstream and downstream from the center of each regulatory element [48]. This implies that the ends of the looping segment are non-chromatinized dsDNA, while the looping segment itself may be chromatinized. We argue that our model may be applied also for this case, provided that the looping segment is contained within a blob. This is because the eclipse effect is a result of the loss of correlation between the two chain termini. Thus, the effect should occur for any sufficiently-long chain ($L_{chain} \gg b_{chain}$), independent of the exact chain parameters ($L_{chain}$, $b_{chain}$, $w_{chain}$, etc.). The effect is sensitive to the TF size and location, and to the looping criteria. However, these are assumed to equal the conditions of non-chromatinized DNA at the chain termini (i.e. in close proximity to the enhancer and promoter).

We calculated typical blob sizes for a few model organisms (see S1 File Section 2). For bacteria, there are few examples of looping with lengths considered in this work, while the vast majority of the loops are short and are covered by the model described previously [28]. For *D. melanogaster*, a typical blob contains many kbp of chromatinized DNA. Thus our model may be applicable to enhancer-promoter systems in *D. melanogaster* and other organisms with low chromatin volume fractions, and to the *eve* 3/7 enhancer in particular.

For enhancer-promoter systems for which a non-interacting blob cannot be assumed (small blob size due to high chromatin volume fraction, or very long looping segment), we must consider the interaction of the looping segment with the rest of the chromosome. Recent results regarding chromatin structure [34] indicate that regions within eukaryotic chromosomes are unentangled but do interact (for example, by confining each other sterically). We attempted to simulate such confinement using a hard-wall sphere around the simulated chains. We found that the probability of looping is increased by confinement. This is perhaps not surprising, since regions of the order of 1 Mbp within chromosomes have been found to interact

with a contact probability with power-law constant $\sim$-1 [34, 44], as compared to the $\sim$-1.5 prediction of the equilibirum globule model [8]. This behavior can be explained by the formation of self-organized non-entangled regions, which can form via a variety of mechanisms [45, 46, 49, 50]. Unlike the looping probability, the eclipse effect was found to be unaffected by confinement, up to the minimal confining sphere size that we were able to simulate. Note that the simulation dimensions are scalable: if we scale the bare dsDNA parameters by $\alpha = 10/4.8$, the $10^4$-link simulation confined by a sphere of radius $r$ also describes a polymer with width of $\alpha w = 10$ nm, length of $\alpha L \approx 6800$ nm, and persistence length of $\alpha l_p \approx 110$ nm, which is comparable to $\sim$100 kbp of 10 nm chromatin fiber confined in a sphere of radius $\alpha r$, if we assume a density of 15 bp/nm for the fiber [51]. The range of confining radii and chain lengths corresponds to polymer volume fractions of up to 0.2%. Despite being limited to low volume fractions, the result that the eclipse effect is independent on volume fraction suggests that our model might be applicable to chromatinized enhancer-promoter looping segments that extend beyond the blob size.

Our work indicates that we should consider three ranges for the physics of looping of chromatinized DNA. For short ranges which we studied previously [14, 28], looping is dominated by elastic energy. As shown in this work, there is an intermediate entropic looping range of up to $\sim$10 kbp of non-chromatinized DNA (or $\sim$100 kbp of partially-chromatinized DNA). Recent studies indicate that there may be an additional long-range regime in which interactions between neighboring regions of the globular DNA must be taken into account [34, 46].

## Supporting Information

**S1 File. Contains: extended materials and methods, a discussion of blob sizes for model organisms, and the estimation of the bias in the expectation value of the looping probability.**
(PDF)

## Author Contributions

**Conceptualization:** YP SG RA.

**Data curation:** YP.

**Formal analysis:** YP SG RA.

**Funding acquisition:** RA.

**Investigation:** YP.

**Methodology:** YP SG RA.

**Project administration:** RA.

**Resources:** RA.

**Software:** YP.

**Supervision:** RA.

**Validation:** YP SG RA.

**Visualization:** YP SG RA.

**Writing – original draft:** YP SG RA.

**Writing – review & editing:** YP SG RA.

## References

1. Marko JF, Siggia ED. Stretching DNA. Macromolecules. 1995; 28(26):8759–8770.
2. Müller J, Oehler S, Müller-Hill B. Repression of lac Promoter as a Function of Distance, Phase and Quality of an Auxiliary lac Operator. Journal of Molecular Biology. 1996; 257(1):21–29. doi: 10.1006/jmbi.1996.0143 PMID: 8632456
3. Cloutier TE, Widom J. DNA twisting flexibility and the formation of sharply looped protein-DNA complexes. Proceedings of the National Academy of Sciences. 2005; 102(10):3645–3650. PMID: 15718281
4. Wiggins PA, van der Heijden T, Moreno-Herrero F, Spakowitz A, Phillips R, Widom J, et al. High flexibility of DNA on short length scales probed by atomic force microscopy. Nature Nanotechnology. 2006; 1(2):137–141. doi: 10.1038/nnano.2006.63 PMID: 18654166
5. Vafabakhsh R, Ha T. Extreme Bendability of DNA Less than 100 Base Pairs Long Revealed by Single-Molecule Cyclization. Science. 2012; 337(6098):1097–1101. doi: 10.1126/science.1224139 PMID: 22936778
6. Jacobson H, Stockmayer WH. Intramolecular Reaction in Polycondensations. I. The Theory of Linear Systems. The Journal of Chemical Physics. 1950; 18(12):1600–1606. doi: 10.1063/1.1747547
7. Flory PJ. Statistical Mechanics of Chain Molecules. Interscience Publishers; 1969.
8. Gennes PG. Scaling Concepts in Polymer Physics. Ithaca, NY: Cornell University Press; 1979. doi: 10.1063/1.2914118
9. Shimada J, Yamakawa H. Ring-closure probabilities for twisted wormlike chains. Application to DNA. Macromolecules. 1984; 17(4):689–698. doi: 10.1021/ma00134a028
10. Crothers DM, Drak J, Kahn JD, Levene SD. DNA bending, flexibility, and helical repeat by cyclization kinetics. In: David M J Lilley JED, editor. Methods in Enzymology. vol. Volume 212 of DNA Structures Part B: Chemical and Electrophoretic Analysis of DNA. Academic Press; 1992. p. 3–29. doi: 10.1016/0076-6879(92)12003-9 PMID: 1518450
11. Yan J, Kawamura R, Marko JF. Statistics of loop formation along double helix DNAs. Physical Review E. 2005; 71(6):061905. doi: 10.1103/PhysRevE.71.061905 PMID: 16089763
12. Buck M, Gallegos MT, Studholme DJ, Guo Y, Gralla JD. The Bacterial Enhancer-Dependent σ54 Transcription Factor. Journal of Bacteriology. 2000; 182(15):4129–4136. PMID: 10894718
13. Su W, Porter S, Kustu S, Echols H. DNA-looping and enhancer activity: association between DNA-bound NtrC activator and RNA polymerase at the bacterial glnA promoter. Proceedings of the National Academy of Sciences of the United States of America. 1990; 87(14):5504–5508. doi: 10.1073/pnas.87.14.5504 PMID: 2164685
14. Amit R, Garcia HG, Phillips R, Fraser SE. Building Enhancers from the Ground Up: A Synthetic Biology Approach. Cell. 2011; 146(1):105–118. doi: 10.1016/j.cell.2011.06.024 PMID: 21729783
15. Davidson EH. The Regulatory Genome. Elsevier; 2006.
16. Gray S, Szymanski P, Levine M. Short-range repression permits multiple enhancers to function autonomously within a complex promoter. Genes & Development. 1994; 8(15):1829–1838. doi: 10.1101/gad.8.15.1829 PMID: 7958860
17. Gray S, Levine M. Short-range transcriptional repressors mediate both quenching and direct repression within complex loci in Drosophila. Genes & Development. 1996; 10(6):700–710. doi: 10.1101/gad.10.6.700 PMID: 8598297
18. Arnosti DN, Barolo S, Levine M, Small S. The eve stripe 2 enhancer employs multiple modes of transcriptional synergy. Development. 1996; 122(1):205–214. PMID: 8565831
19. Arnosti DN, Gary S, Barolo S, Zhou J, Levine M. The gap protein knirps mediates both quenching and direct repression in the Drosophila embryo. The EMBO Journal. 1996; 15(14):3659–3966. PMID: 8670869
20. Nibu Y, Zhang H, Levine M. Interaction of Short-Range Repressors with Drosophila CtBP in the Embryo. Science. 1998; 280(5360):101–104. doi: 10.1126/science.280.5360.101 PMID: 9525852
21. Nibu Y, Zhang H, Bajor E, Barolo S, Small S, Levine M. dCtBP mediates transcriptional repression by Knirps, Krüppel and Snail in the Drosophila embryo. The EMBO Journal. 1998; 17(23):7009–7020. doi: 10.1093/emboj/17.23.7009 PMID: 9843507
22. Strunk B, Struffi P, Wright K, Pabst B, Thomas J, Qin L, et al. Role of CtBP in Transcriptional Repression by the Drosophila giant Protein. Developmental Biology. 2001; 239(2):229–240. doi: 10.1006/dbio.2001.0454 PMID: 11784031
23. Struffi P, Arnosti DN. Functional Interaction between the Drosophila Knirps Short Range Transcriptional Repressor and RPD3 Histone Deacetylase. Journal of Biological Chemistry. 2005; 280(49):40757–40765. doi: 10.1074/jbc.M506819200 PMID: 16186109

24. Spain MM, Caruso JA, Swaminathan A, Pile LA. Drosophila SIN3 Isoforms Interact with Distinct Proteins and Have Unique Biological Functions. Journal of Biological Chemistry. 2010; 285(35):27457–27467. doi: 10.1074/jbc.M110.130245 PMID: 20566628

25. Keller SA, Mao Y, Struffi P, Margulies C, Yurk CE, Anderson AR, et al. dCtBP-Dependent and -Independent Repression Activities of the Drosophila Knirps Protein. Molecular and Cellular Biology. 2000; 20 (19):7247–7258. doi: 10.1128/MCB.20.19.7247-7258.2000 PMID: 10982842

26. Ryu JR, Arnosti DN. Functional similarity of Knirps CtBP-dependent and CtBP-independent transcriptional repressor activities. Nucleic Acids Research. 2003; 31(15):4654–4662. doi: 10.1093/nar/gkg491 PMID: 12888527

27. Mannervik M, Levine M. The Rpd3 histone deacetylase is required for segmentation of the Drosophila embryo. Proceedings of the National Academy of Sciences of the United States of America. 1999; 96 (12):6797–6801. doi: 10.1073/pnas.96.12.6797 PMID: 10359792

28. Brunwasser-Meirom M, Pollak Y, Goldberg S, Levy L, Atar O, Amit R. Using synthetic bacterial enhancers to reveal a looping-based mechanism for quenching-like repression. Nature Communications. 2016; 7:10407. doi: 10.1038/ncomms10407 PMID: 26832446

29. Pollak Y, Goldberg S, Amit R. Self-avoiding wormlike chain model for double-stranded-DNA loop formation. Physical Review E. 2014; 90(5):052602. doi: 10.1103/PhysRevE.90.052602 PMID: 25493808

30. Chen ZY, Noolandi J. Renormalization-group scaling theory for flexible and wormlike polymer chains. The Journal of Chemical Physics. 1992; 96(2):1540–1548. doi: 10.1063/1.462138

31. Tree DR, Muralidhar A, Doyle PS, Dorfman KD. Is DNA a Good Model Polymer? Macromolecules. 2013; 46(20):8369–8382. doi: 10.1021/ma401507f

32. Glotzer SC, Paul W. Molecular and Mesoscale Simulation Methods for Polymer Materials. Annual Review of Materials Research. 2002; 32(1):401–436. doi: 10.1146/annurev.matsci.32.010802.112213

33. Kotelyanskii M, Theodorou DN. Simulation Methods for Polymers. 1st ed. New York: CRC Press; 2004.

34. Lieberman-Aiden E, van Berkum NL, Williams L, Imakaev M, Ragoczy T, Telling A, et al. Comprehensive mapping of long-range interactions reveals folding principles of the human genome. Science (New York, NY). 2009; 326(5950):289–293. doi: 10.1126/science.1181369 PMID: 19815776

35. Vettorel T, Grosberg AY, Kremer K. Statistics of polymer rings in the melt: a numerical simulation study. Physical Biology. 2009; 6(2):025013. doi: 10.1088/1478-3975/6/2/025013 PMID: 19571364

36. Halverson JD, Smrek J, Kremer K, Grosberg AY. From a melt of rings to chromosome territories: the role of topological constraints in genome folding. Reports on Progress in Physics. 2014; 77(2):022601. doi: 10.1088/0034-4885/77/2/022601 PMID: 24472896

37. Rosenbluth MN, Rosenbluth AW. Monte Carlo Calculation of the Average Extension of Molecular Chains. The Journal of Chemical Physics. 1955; 23(2):356–359. doi: 10.1063/1.1741967

38. Struffi P, Corado M, Kaplan L, Yu D, Rushlow C, Small S. Combinatorial activation and concentration-dependent repression of the Drosophila even skipped stripe 3+7 enhancer. Development. 2011; 138 (19):4291–9. doi: 10.1242/dev.065987 PMID: 21865322

39. Maeshima K, Kaizu K, Tamura S, Nozaki T, Kokubo T, Takahashi K. The physical size of transcription factors is key to transcriptional regulation in chromatin domains. Journal of Physics: Condensed Matter. 2015; 27(6):064116. doi: 10.1088/0953-8984/27/6/064116 PMID: 25563431

40. Perissi V, Jepsen K, Glass CK, Rosenfeld MG. Deconstructing repression: evolving models of co-repressor action. Nature Reviews Genetics. 2010; 11(2):109–123. doi: 10.1038/nrg2736 PMID: 20084085

41. Janssens H, Hou S, Jaeger J, Kim AR, Myasnikova E, Sharp D, et al. Quantitative and predictive model of transcriptional control of the Drosophila melanogaster even skipped gene. Nat Genet. 2006; 38 (10):1159–65. doi: 10.1038/ng1886 PMID: 16980977

42. Segal E, Raveh-Sadka T, Schroeder M, Unnerstall U, Gaul U. Predicting expression patterns from regulatory sequence in Drosophila segmentation. Nature. 2008; 451(7178):535–40. doi: 10.1038/nature06496 PMID: 18172436

43. Kim AR, Martinez C, Ionides J, Ramos AF, Ludwig MZ, Ogawa N, et al. Rearrangements of 2.5 kilobases of noncoding DNA from the Drosophila even-skipped locus define predictive rules of genomic cis-regulatory logic. PLoS Genet. 2013; 9(2):e1003243. doi: 10.1371/journal.pgen.1003243 PMID: 23468638

44. Duan Z, Andronescu M, Schutz K, McIlwain S, Kim YJ, Lee C, et al. A three-dimensional model of the yeast genome. Nature. 2010; 465(7296):363–367. doi: 10.1038/nature08973 PMID: 20436457

45. Barbieri M, Chotalia M, Fraser J, Lavitas LM, Dostie J, Pombo A, et al. Complexity of chromatin folding is captured by the strings and binders switch model. Proceedings of the National Academy of Sciences. 2012; 109(40):16173–16178. doi: 10.1073/pnas.1204799109 PMID: 22988072

46. Goloborodko A, Marko JF, Mirny LA. Chromosome Compaction by Active Loop Extrusion. Biophysical Journal. 2016; 110(10):2162–2168. doi: 10.1016/j.bpj.2016.02.041 PMID: 27224481

47. Khokhlov AR, Grosberg AY, Pande VS. Statistical Physics of Macromolecules. 1994th ed. New York: American Institute of Physics; 2002.

48. Heintzman ND, Stuart RK, Hon G, Fu Y, Ching CW, Hawkins RD, et al. Distinct and predictive chromatin signatures of transcriptional promoters and enhancers in the human genome. Nature Genetics. 2007; 39(3):311–318. doi: 10.1038/ng1966 PMID: 17277777

49. Grosberg AY, Nechaev SK, Shakhnovich EI. The role of topological constraints in the kinetics of collapse of macromolecules. Journal de Physique. 1988; 49(12):2095–2100. doi: 10.1051/jphys:0198800490120209500

50. Grosberg A, Rabin Y, Havlin S, Neer A. Crumpled Globule Model of the Three-Dimensional Structure of DNA. EPL (Europhysics Letters). 1993; 23(5):373. doi: 10.1209/0295-5075/23/5/012

51. Walhout M, Vidal M, Dekker J, editors. Handbook of Systems Biology: Concepts and Insights. 1st ed. London: Academic Press; 2012.